JOURNAL OF GEOPHYSICAL RESEARCH, VOL. 106, NO. D17, PAGES 20,025–20,043, SEPTEMBER 16, 2001

Tropical teleconnection and local response to SST anomalies during the 1997-1998 El Niño

Hui Su, J. David Neelin,[1] and Chia Chou[2]

Department of Atmospheric Sciences, University of California, Los Angeles, California

Abstract. The quasi-equilibrium tropical circulation model (QTCM) is used to examine the response to various sea surface temperature (SST) anomalies in the tropical oceans during the 1997-1998 El Niño. Both local and remote responses are noted. The negative precipitation anomalies to the north and south of the El Niño - Southern Oscillation (ENSO) enhanced precipitation region are largely a response to the warm SST anomalies in the central and eastern Pacific. However, in the western Pacific and maritime continent, reduction of rainfall is mainly caused by local cold SST anomalies. In the winter of the 1997-1998 El Niño, strong warm SST anomalies in the Indian Ocean contributed to the local enhanced rainfall. They affect precipitation anomalies in central, eastern, and southern Africa. The drought in northern South America is clearly a remote response to ENSO warm SST anomalies in the Pacific, while the SST anomalies in the Atlantic also impact the drought. The tropical Pacific cold SST anomalies surrounding the ENSO warm anomalies appear not to be caused by surface flux changes associated with atmospheric teleconnection (in simulations with specified SST in the ENSO warm region and a mixed-layer ocean model elsewhere). Atmospheric circulation tends to spread the warm anomalies, but ocean dynamics appears also to be important for both cold and warm SST anomalies outside the equatorial upwelling region. In both the regional specified SST experiments and mixed-layer experiments, relative subsidence tends to occur within convective zones, and it is generally localized. On the other hand, tropospheric temperature and wind anomalies spread much farther. The typical spatial scale of the remote response in temperature and wind fields tends to be larger than the dominant scale of the precipitation response. The remote response in precipitation anomalies does not appear to be related to temperature and wind anomalies in a simple manner.

1. Introduction

On the interannual timescale, El Niño - Southern Oscillation (ENSO) dominates the variability in the atmosphere and ocean circulations [*Wallace et al.,* 1998; *Trenberth et al.,* 1998]. Tropical precipitation anomalies associated with El Niño include drought in northern South America, greater than normal precipitation in the eastern equatorial Africa, and drier than normal conditions in Australia [*Ropelewski and Halpert,* 1987]. Within the tropical Pacific, reduction of rainfall in the western Pacific and Indonesian region is noted [*Quinn et al.,* 1978]. Moreover, there are negative precipitation anomalies in the vicinity of the El Niño enhanced precipitation region to the north and south [*Ropelewski and Halpert,* 1987]. Thus a "horseshoe" shape of negative precipitation anomalies is observed. Interestingly, cold SST anomalies also tend to occur in a "horseshoe" pattern surrounding the ENSO warm anomaly in the tropical Pacific [*Wallace et al.,* 1998]. However, the relationship between the cold SST anomalies and the negative rainfall anomalies is not clear. During El Niño years, SSTs in other tropical oceans often experience large variations as well [*Halpert and Ropelewski,* 1992; *Wallace et al.,* 1998]. Both teleconnection from the main El Niño warm anomalies and the SST anomalies in other ocean basins can potentially affect the rainfall over the oceans and adjacent continents.

There are a large number of studies using general circulation models (GCMs) to simulate the atmospheric response to tropical SST anomalies on seasonal and interannual timescales [*Lau,* 1985; *Barnett et al.,* 1994; *Sud et al.,* 1991; *Janicot et al.,* 1998; *Kumar and Ho-*

[1]Also at Institute of Geophysics and Planetary Physics, University of California, Los Angeles.

[2]Now at Department of Atmospheric Sciences, Chinese Culture University, Taipei, Taiwan.

Paper number 2000JD000124.
0148-0227/01/2000JD000124$09.00

erling, 1998; *Mechoso et al.,* 1987; *Farrara et al.,* 2000; *Barnston et al.,* 1999a, 1999b; *Rowell,* 1998; *Goddard and Graham,* 1999; *Chang et al.,* 2000; *Saravanan and Chang,* 2000; *Latif et al.,* 1999; *Venzke et al.,* 2000]. Studies using SST anomalies restricted to the Pacific basin find repeated tropical response as well as midlatitude teleconnection. Other studies focus on particular regions and impacts of the Indian Ocean and the Atlantic Ocean SSTs. For example, it was found that Indian Ocean SST anomalies have significant impacts on the rainfall anomalies over eastern and southern Africa [*Goddard and Graham,* 1999], while west Africa monsoon dynamics are greatly affected by anomalies of SST in the equatorial Atlantic and Pacific [*Janicot et al.,* 1998; *Palmer,* 1986; *Folland et al.,* 1986].

In this study we use an intermediate atmospheric model, known as the quasi-equilibrium tropical circulation model (QTCM), to perform similar SST response experiments, in this case systematically subdividing temporal SST anomalies into particular regions. The 1997-1998 El Niño event is chosen as an example because it was one of the strongest events on record. Strong warming of SST also occurred in the Indian Ocean. Rainfall anomalies and tropospheric temperature and wind anomalies are examined and compared with National Centers for Environmental Prediction (NCEP)/National Center for Atmospheric Research (NCAR) reanalysis data [*Kalnay et al.,* 1996]. Compared to a GCM, the QTCM is very economical to run and analyze, permitting a large number of ensemble experiments. Work with the QTCM can complement analogous GCM studies. On the one hand, we evaluate the model's capability of performing such climate-related studies by comparing the model results with NCEP/NCAR reanalysis data and other GCM results. This will provide background for subsequent theoretical studies built down from the intermediate model. A recent study by *Frederiksen et al.* [2001] found that using observed SSTs in an atmospheric GCM could simulate and predict tropical anomalies in the 1997-1998 El Niño. This provides extra confidence that models forced with observed SSTs can be used to diagnose causes of precipitation anomalies. On the other hand, we aim to examine local versus remote effects via teleconnections in the atmosphere between the basins; for instance, whether the negative precipitation anomaly near the intense warming area in the tropical Pacific is induced by the warming of SST in the central and eastern Pacific or forced by local negative SST anomalies. Similarly, we examine the effects of SST anomalies in the Indian and Atlantic Oceans and compare them with those in the Pacific Ocean. Moreover, we perform simulations with all tropical SST anomalies or a combination of subregions of the tropical oceans. The sum of results from the SST anomalies specified in individual areas is compared with results from runs where SST anomalies are specified in all regions to test to what degree the SST response is linear.

Furthermore, we aim to investigate the extent to which the SST warming is translated into tropospheric temperature and wind anomalies and how they are related to precipitation anomalies. The scales of teleconnection in temperature, wind field, and precipitation are sought.

A caveat that applies to all teleconnection studies, based on only an atmospheric model, is that changes in oceanic circulation induced, for instance, by a teleconnected circulation anomaly, can feed back on the atmospheric circulation. The results from an atmosphere-only model with specified oceanic boundary conditions may differ significantly from the results from a coupled atmosphere-ocean model [*Kumar and Hoerling,* 1998]. In some of the results presented here, the source of the SST anomalies remains ambiguous, although we can associate part of the atmospheric response with a specific region of SST anomalies. One step toward coupling is taken in some experiments using a slab mixed-layer ocean model. This can serve to point to effects on SST of teleconnected surface heat flux anomalies. The role of changes in oceanic circulation, which can be potentially important [*Webster et al.,* 1999], is not directly addressed. In some cases the lack of anomalies in the atmosphere/mixed-layer model may provide circumstantial evidence for the importance of ocean circulation.

The structure of this paper is as follows: Section 2 briefly describes the physical packages used in the model and the design of model experiments. Section 3 presents model results, including overall El Niño variability, response to various SST anomalies, and a preliminary simulation of the QTCM coupled with a slab mixed-layer ocean model. Summary and conclusions are given in section 4.

2. Summary of the QTCM

The quasi-equilibrium tropical circulation model is an intermediate complexity atmospheric circulation model. The constraints placed on the flow by quasi-equilibrium convective parameterization are used to calculate typical vertical structures of temperature, moisture, and winds. These are used in a truncated Galerkin representation for computational efficiency and to promote theoretical understanding. The model includes nonlinear advection and cloud-radiation feedback, a simple land-atmosphere model and Betts-Miller cumulus parameterization. Detailed model description and evaluation of simulations can be found in the works of *Neelin and Zeng* [2000] and *Zeng et al.* [2000]. While the limited vertical structure precludes simulations of some aspects of tropical flow that could be captured in GCMs, the QTCM simulates many features of tropical seasonal to interannual variability, including ENSO anomalies. For example, composites of simulated ENSO rainfall anomalies agree well with observations [*Zeng et al.,* 2000, Figures 17 and 18]. The model has been used to

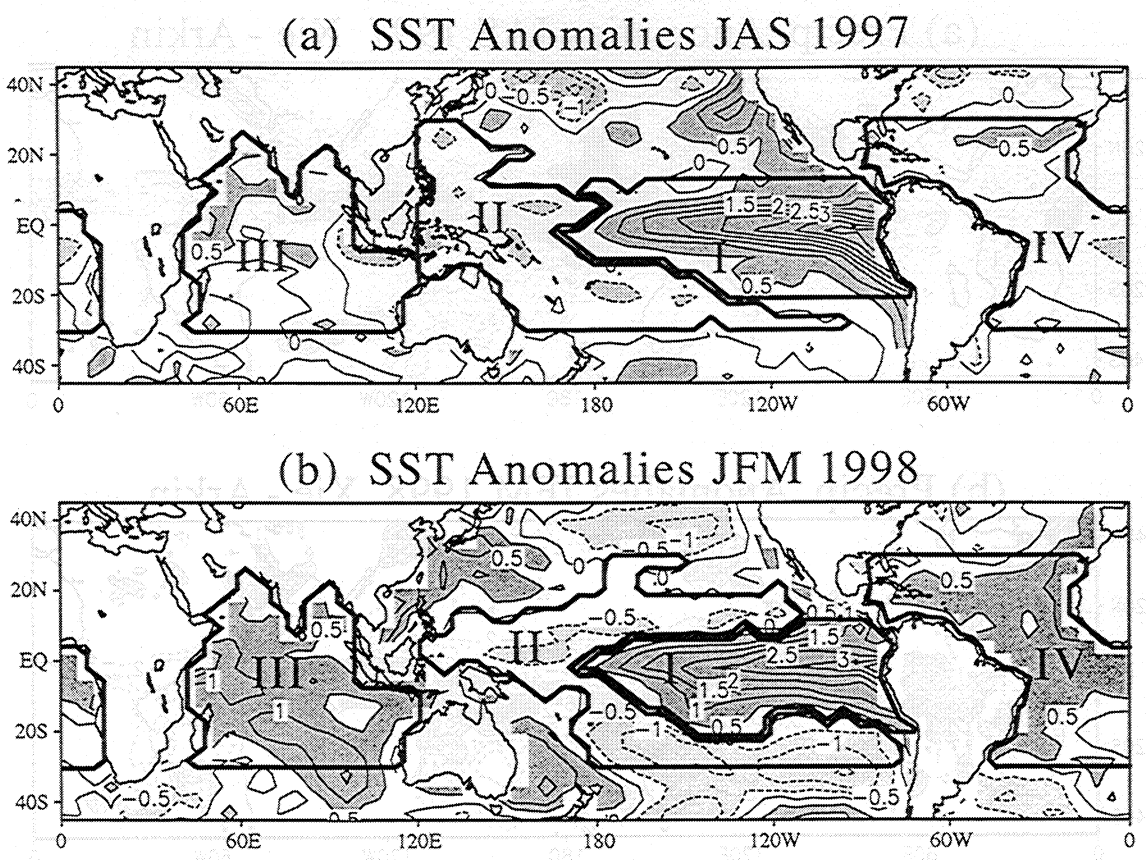

Figure 1. Sea surface temperature anomalies (Celsius) for (a) July-September 1997 and (b) January-March 1998. Contour interval is 0.5°C with dark shading above 0.5°C and light shading below −0.5°C. Negative contours are dashed. The areas marked as I-IV represent the regions for specific SST anomaly experiments: POSPAC (I), NEGPAC (II), IND (III), and ATL (IV).

study the Madden-Julian Oscillation [*Lin et al.,* 2000] and stochastic modeling of tropical convection [*Lin and Neelin,* 2000]. *Chou et al.* [2001] used it in idealized settings to investigate the physical processes impacting the magnitude and propagation of monsoon. In this study we use QTCM1 version 2.1 with the nonlinear calculation of the convective reference profile option chosen.

In this study, most experiments are conducted with specified SSTs as lower boundary forcing. In one case, a slab-mixed layer ocean model is coupled with the QTCM to test the effect of atmospheric teleconnections on the SST distribution. A fixed mixed-layer depth of 50 m is used for simplicity. The divergence of ocean transport is parameterized using the "Q-flux" correction scheme [*Hansen et al.,* 1988, 1997] where time-averaged surface heat fluxes balance the ocean transport. The Q-flux is obtained from a control run with specified climatological SST. Climatological Q-flux is diagnosed from the seasonal surface fluxes and the time rate of change of SST in the control run. The mixed-layer model interacts with the atmosphere via daily averaged SST and surface fluxes. Our model domain is from 60°S to 60°N, with a resolution of 5.625° x 3.75°.

For the prescribed SST experiments, we focus on anomalies from the tropical oceans, excluding anomalies outside 30°S-30°N. Two types of simulations are performed. The first one runs from January 1982 to December 1998 using time-varying observed SST [*Reynolds and Smith,* 1994]. Anomalous fields from July-September (JAS) 1997 and January-March (JFM) 1998 with respect to climatological annual cycle for 1982 to 1998 are compared with corresponding NCEP/NCAR reanalysis data. The other set of experiments uses SST with anomalies specified in particular regions. For each SST distribution, 10 integrations from May to September 1997 or from November 1997 to March 1998 are conducted using slightly different initial conditions. Anomalies for JAS 1997 and JFM 1998 are obtained by subtracting the ensemble means for the 10 control experiments, in which climatological SST is used, from the ensemble means for the 10 integrations using a specific SST distribution. The 10 different initial conditions are obtained from a 10 year integration using seasonal SST. The thermodynamical and dynamical variables at the end of each year are saved as one of the initial conditions for ensemble integrations. The members of the ensemble tend to have similar signals, suggesting the SST response is a substantial component. We chose several SST patterns: the experiment denoted OBS-SST includes the full observed SST anomalies, POSPAC in-

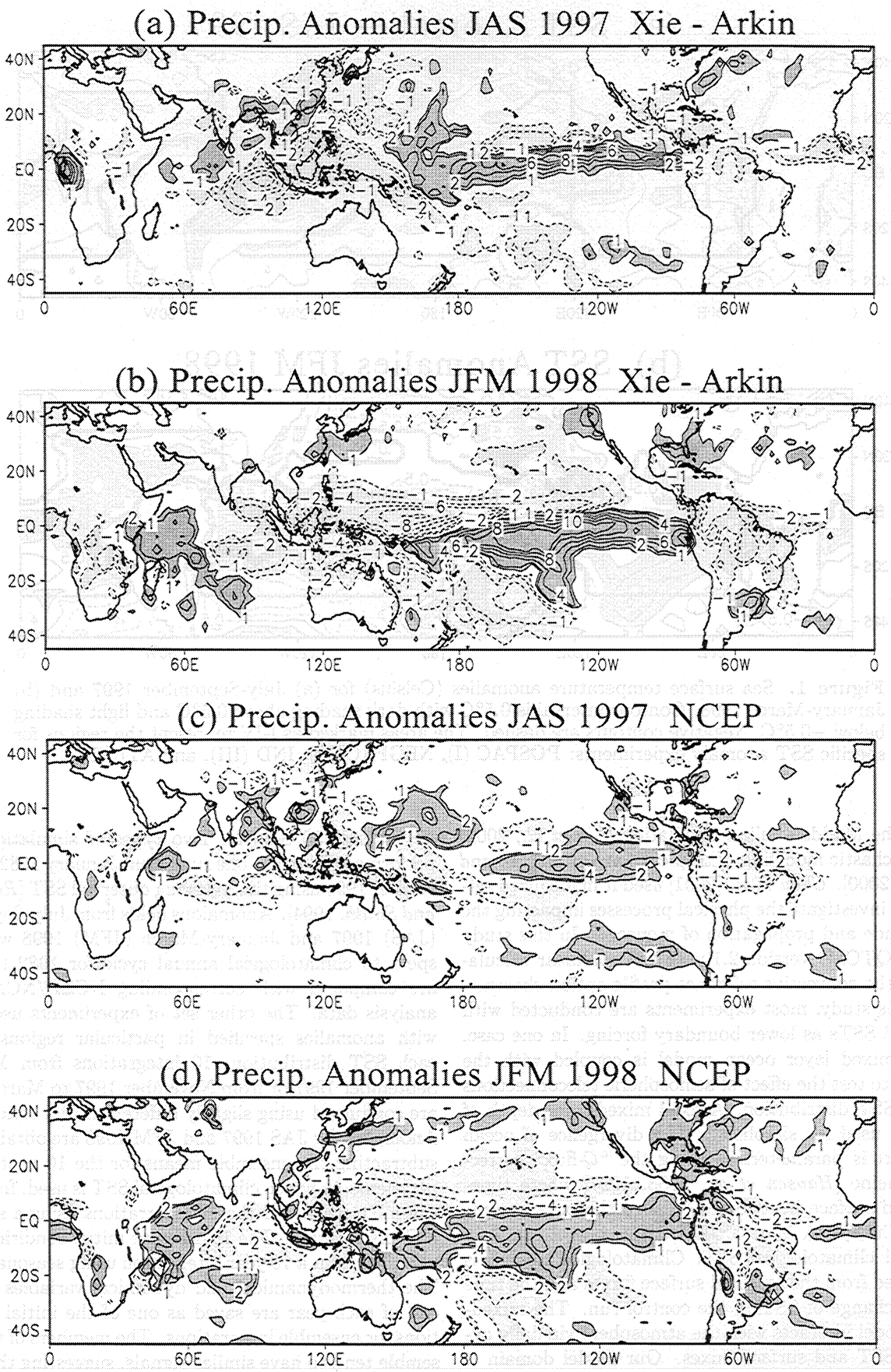

Figure 2. Precipitation anomalies from Xie and Arkin for (a) JAS 1997 and (b) JFM 1998 and from NCEP/NCAR reanalysis (c) JAS 1997 and (d) JFM 1998. Contours are at -8, -6, -4, -2, -1, 1, 2, 4, 6, 8, 10 mm d^{-1}, with dark shading above 1 mm d^{-1} and light shading below -1 mm d^{-1}. Negative contours are dashed.

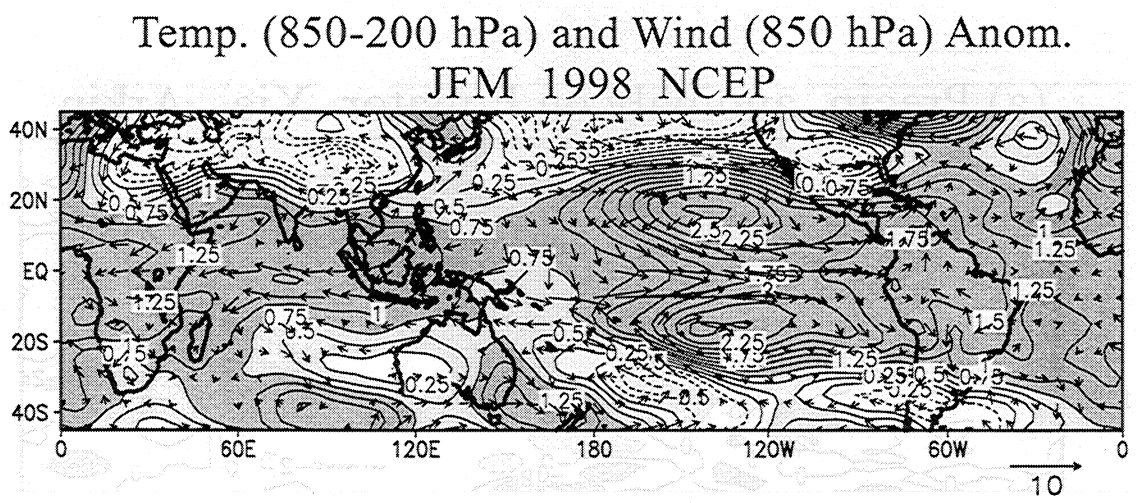

Figure 3. Tropospheric averaged (850-200 hPa) temperature anomalies and 850 hPa wind anomalies for JFM 1998 from NCEP/NCAR reanalysis. Contours are temperature anomalies with an interval of 0.25°C, dark shading above 0.75 and light shading between 0.25 and 0.75. Negative contours are dashed. Wind vectors are in m s^{-1}.

cludes only the positive SST anomalies in the tropical Pacific Ocean, NEGPAC includes only the negative SST anomalies in the tropical Pacific Ocean, IND includes only the SST anomalies in the Indian Ocean, ATL includes only the SST anomalies in the Atlantic Ocean, PAC includes SST anomalies (both signs) in the Pacific Ocean, and PACSTAR is the complement of PAC since it includes the SST anomalies outside the Pacific Ocean. Figure 1 shows the respective areas for each specific SST anomaly run.

3. Model Results

3.1. Model-Simulated ENSO Variability

During the 1997-1998 ENSO event, anomalous SST warming was evident both in the summer and in the winter seasons. To fully illustrate the characteristics of this ENSO event, we examine the variability of both seasons. Figure 1 exhibits the observed SST anomalies averaged over the 1997 summer (JAS, Figure 1a) and the 1998 winter (JFM, Figure 1b). In boreal summer of 1997, the warm anomaly was mainly in the central and eastern Pacific. Relatively small warming up to 0.5°C was observed near the coast of Africa in the western Indian Ocean. The Atlantic had only small anomalies. However, both the Indian and the Atlantic Oceans displayed broad warming during JFM 1998. The SST anomalies were more than 1°C in the western and the southern Indian Ocean. In the western Pacific, SST was colder than normal in both seasons. To the east of the dateline, warm anomalies were flanked by relatively weak cold anomalies.

Associated with the SST anomalies, the precipitation field showed strong anomalous signals. Figure 2 shows the observed precipitation anomalies from *Xie and Arkin* [1997] during JAS 1997 and JFM 1998. For comparison the corresponding NCEP/NCAR reanalysis of precipitation anomaly is given in Figures 2c and 2d. In both JAS 1997 and JFM 1998, enhanced precipitation extended from 160°E to the coast of Peru near the equator over the anomalously warm Pacific Ocean. In the summer of 1997 the precipitation anomalies near the dateline were extended somewhat north and south. Negative precipitation anomalies were present in the western Pacific and in narrow areas directly adjacent to the northern and southern boundaries of the enhanced precipitation. During the wintertime, positive rainfall anomalies spread more to the south of equator with a tongue extending to 30°S and west of 120°W. Negative precipitation anomalies in the Pacific were distributed to the north and southwest of the warm area. In JAS 1997, when SST anomalies in the Indian Ocean were relatively small, there were mainly negative rainfall anomalies in the Indian Ocean. In the winter of 1998 the Indian Ocean experienced strong warming. Enhanced precipitation occurred in a broad region of the western Indian Ocean, while the eastern half had less-than-normal rainfall. Reduction of rainfall in the tropical convergence zone over northern South America was evident in both seasons. The rainfall anomalies from the NCEP/NCAR reanalysis are broadly similar to the Xie-Arkin data. However, substantial differences exist, especially over certain ocean regions. For example, the NCEP/NCAR reanalysis had a negative rainfall anomaly at the equator near the dateline during JAS 1997, in contrast to the continuous pattern of positive anomaly in that region in the Xie-Arkin observations. A strip of positive rainfall anomalies of 1-2 mm d^{-1} in the equatorial Atlantic Ocean during JFM 1998 from the NCEP/NCAR reanalysis does not appear in the Xie-Arkin analysis. Such differences between satellite and assimilation data products are useful to bear in mind when comparing the model simulations to either. We focus on the broader features that tend to be robust in examining model teleconnections.

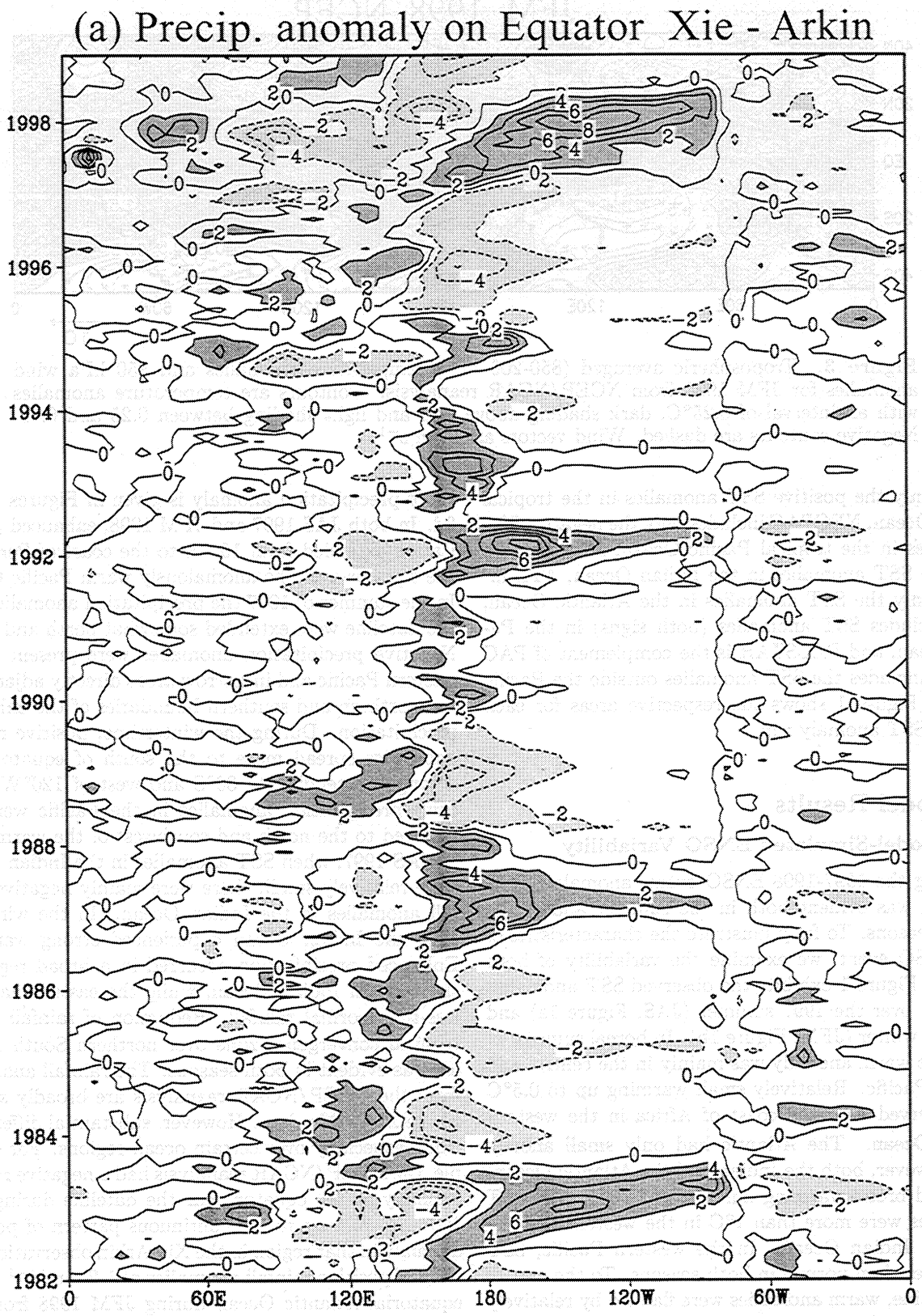

Figure 4. Three month running mean of precipitation anomalies on the equator from January 1982 to December 1998. Contour interval 2 mm d^{-1}, with dark shading above 2 and light shading below -2. (a) Xie-Arkin observations and (b) the model simulation.

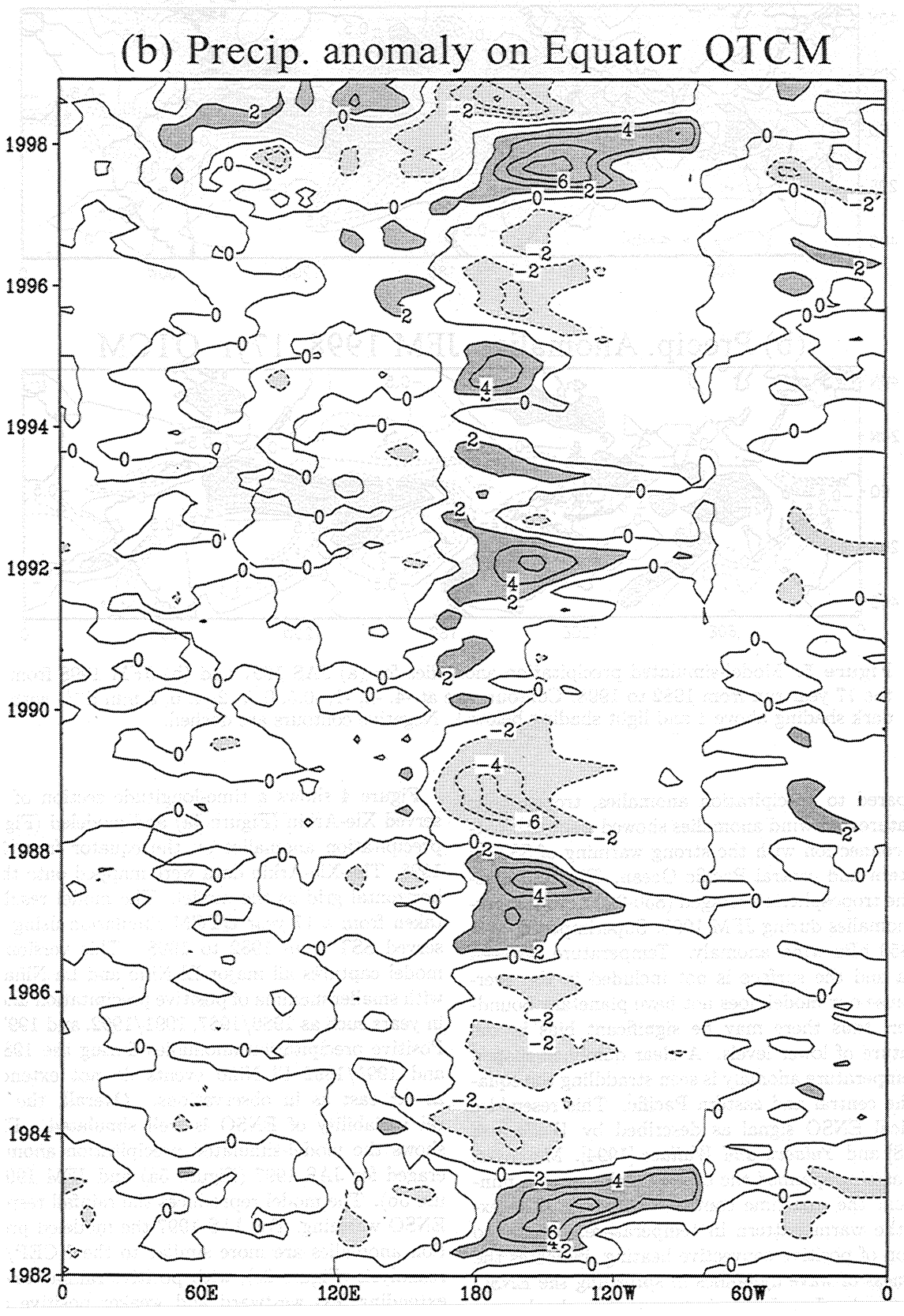

Figure 4 . (continued)

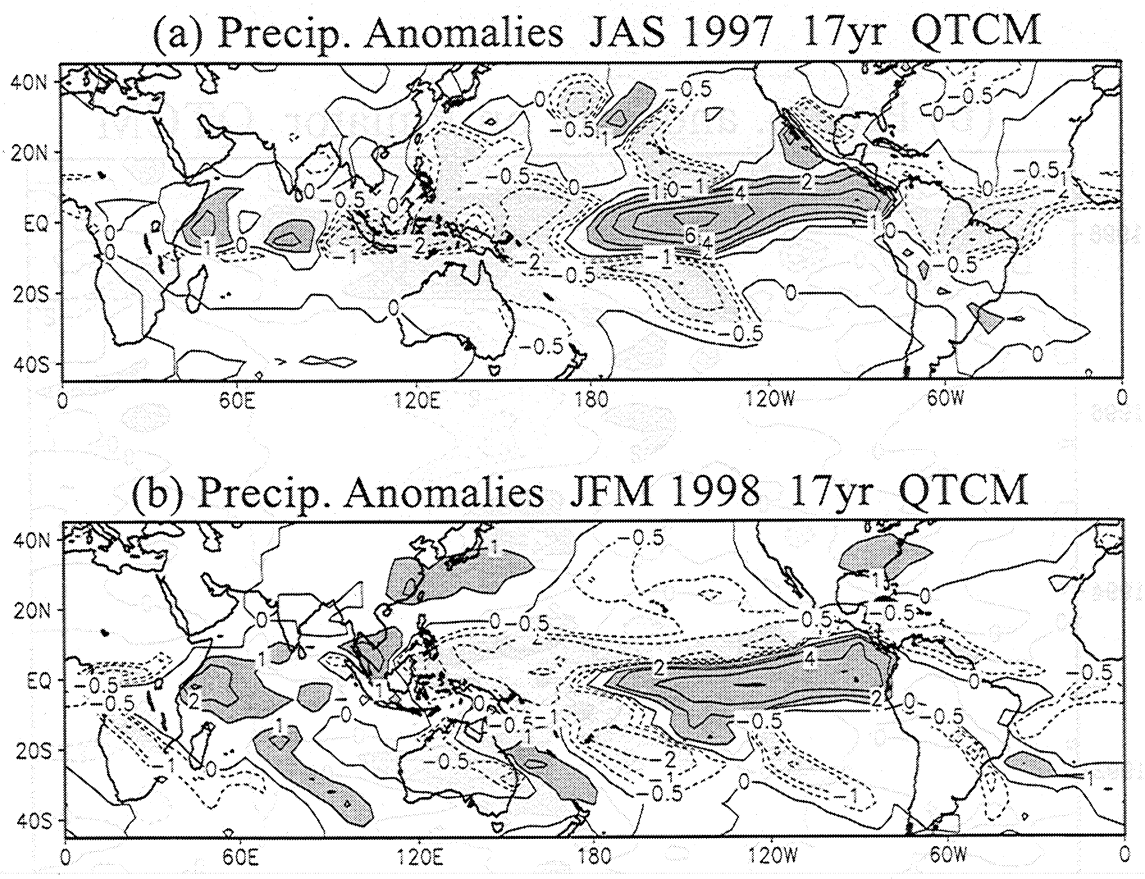

Figure 5. Model-simulated precipitation anomalies for (a) JAS 1997 and (b) JFM 1998 from the 17 year run from 1982 to 1998. Contours are at -4, -2, -1, -0.5, 0, 1, 2, 4, 6, 8 mm d^{-1}, with dark shading above 1 and light shading below 1. Negative contours are dashed.

Compared to precipitation anomalies, tropospheric temperature and wind anomalies showed a smooth pattern in connection with the strong warming of SST in the eastern and central Pacific Ocean. Figure 3 illustrates the tropospheric averaged (850-200 hPa) temperature anomalies during JFM 1998. Superimposed on it is the 850 hPa wind anomaly. Temperature between 850 hPa and the surface is not included in the average because our model does not have planetary boundary layer, thus there may be significant bias in the temperature of lower levels. A clear dumbbell-shaped warm temperature anomaly is seen straddling the equator in the central and eastern Pacific. This resembles the typical ENSO signal as described by *Wallace et al.* [1998] and *Yulaeva and Wallace* [1994]. Moreover, broad warming spanned the entire tropics, with a minimum near the maritime continental region. The extent of the warm pattern in temperature, relative to the region of positive convective heating, indicates the effectiveness of wave dynamics in spreading the ENSO warm anomaly. Low-level wind anomalies also have a large-scale structure, with strong westerly anomalies in the equatorial central and eastern Pacific and easterly anomalies in the Indian Ocean. This is consistent with the large scale of the baroclinic pressure gradient seen in the temperature field.

Figure 4 shows a time-longitude section of the observed Xie-Arkin (Figure 4a) and modeled (Figure 4b) precipitation anomalies on the equator from 1982 to 1998. The Xie-Arkin data were mapped onto the same horizontal grid as the model. The model results were taken from a 17 year QTCM simulation using the observed SST from 1982 to 1998. This version of the model captures all major El Niño and La Niña events with smaller maxima of positive precipitation anomalies in years such as 1986/1987, 1991/1992, and 1997/1998. Positive precipitation anomalies during the 1986/1987 and 1991/1992 El Niño events do not extend quite as far east as in observations. Overall, the temporal variability of ENSO is well simulated. Figure 5 shows the model-simulated precipitation anomaly averaged for JAS 1997 (Figure 5a) and JFM 1998 (Figure 5b). The model reproduces the rainfall response to ENSO warming. For JAS 1997 the modeled precipitation anomalies are more similar to the NCEP/NCAR reanalysis (Figure 2c), with positive rainfall anomalies extending less westward and weaker positive anomalies north of the equator, than to the Xie-Arkin observations (Figure 2a). The reduction of rainfall in South America is captured by the model; however, its areal coverage is much smaller during JFM 1998. In both seasons the model underestimates the nega-

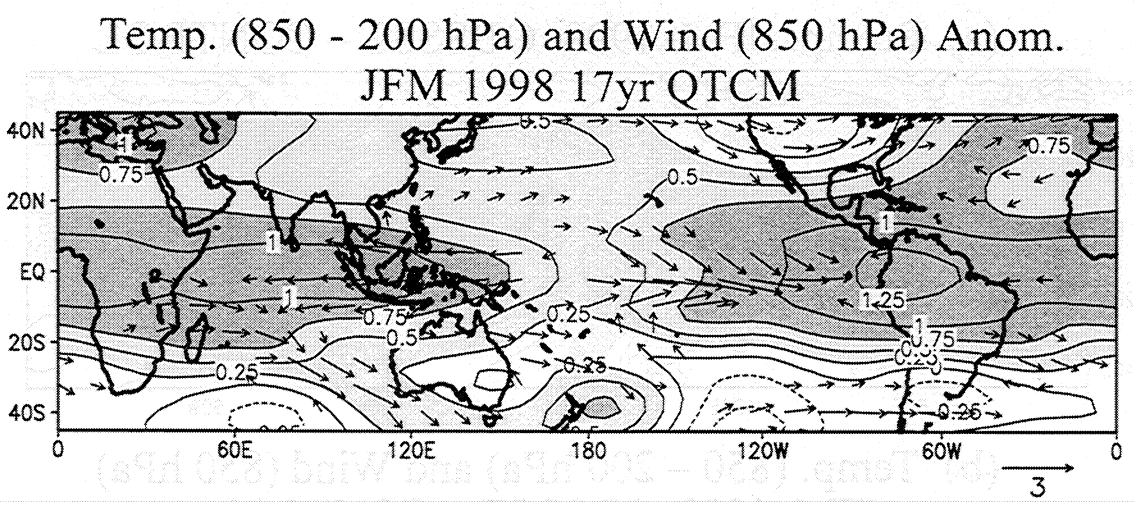

Figure 6. Model-simulated tropospheric averaged (850-200 hPa) temperature anomalies and 850 hPa wind anomalies for JFM 1998 from the 17 year run from 1982 to 1998. Contours and shadings as in Figure 3. Note the wind vector scale is different from Figure 3.

tive rainfall anomalies in the Indian Ocean. Figure 6 displays the model-simulated tropospheric temperature and wind anomalies during JFM 1998 from the 17 year run. Compared to NCEP/NCAR reanalysis (Figure 3), the overall anomalies are smaller in magnitude. The dumbbell-shaped temperature anomalies are shifted eastward with maximum anomalies in the equatorial South America. The shape of warm anomalies qualitatively resembles the traditional wave response to a localized heat source [*Gill,* 1980]. The warm anomalies propagate from the eastern Pacific, across the Atlantic Ocean and Africa, then reach the Indian and western Pacific, with the minimum warming around the dateline. The wind anomalies are consistent with the temperature anomalies. El Niño westerly anomalies are seen in the central and eastern Pacific, while relatively weak easterly anomalies occur in the Atlantic and eastern Indian Oceans. The comparison of tropospheric temperature and wind anomalies during JAS 1997 (figure not shown) between the QTCM simulation and the NCEP/NCAR reanalysis is consistent with that in JFM 1998, although anomalies are generally smaller.

3.2. Response to SST Anomalies in Various Regions

To examine teleconnection versus local response to SST anomalies, we turn to the set of experiments with the observed SST anomalies specified in various subregions. For these experiments, the anomaly of a particular field is defined as the difference between the ensemble means for the specific experiment and the control experiment with climatological SSTs, as described in section 2.

Since the anomaly defined here is different from that for the 17 year integration in the preceding section, Figure 7 shows the simulated anomalous precipitation, tropospheric temperature, and wind anomalies from the run OBS-SST for JFM 1998. Compared to Figures 5b and 6, the anomalies for run OBS-SST are very similar to the 17 year continuous run with observed SST, especially in tropics between 30°S and 30°N. Outside the tropical band, southern Indian Ocean rain band and precipitation in northern China exhibit differences from the 17 year run. Tropospheric temperature and wind anomalies display a slight shift of the storm tracks due to the different climatology state used.

Run POSPAC aims to examine the tropical response to the warm SST anomalies in the tropical Pacific Ocean (30°S-30°N) (anything 8). As expected, it produces strong positive precipitation anomalies locally. Areas of significant negative rainfall anomalies tend to be close to the warm region next to the north and south edges. Compared to Figure 7, the reduction of rainfall in the western Pacific is negligible in run POSPAC, suggesting that it may be caused by local SST anomaly or teleconnection from the Indian Ocean or other parts of the domain. Most of the drought in the Amazon region is reproduced in the POSPAC run. However, the summertime drought is less intense than that in run OBS-SST (figure not shown), while areas of decreased rainfall are concentrated in the equatorial Atlantic Ocean in the winter time, compared to run OBS-SST and observations. This indicates that the Atlantic SST anomaly may contribute to the precipitation anomaly in South America, despite the strong teleconnection from the Pacific warm SST. The positive SST anomaly in the Pacific also produces negative rainfall anomalies up to -1 mm d^{-1} in the Indian Ocean and northern Australia.

In contrast to the precipitation field, tropospheric temperature displays more homogeneous features with maximum warming centered at the coast of Ecuador (Figures 8b and 8d). In JAS 1997 the pattern of the warm temperature anomalies is reminiscent of the classic wave response to a localized heat source [*Gill,* 1980], with symmetric warm anomalies about the equator and a zonally elongated warm anomaly propagating east-

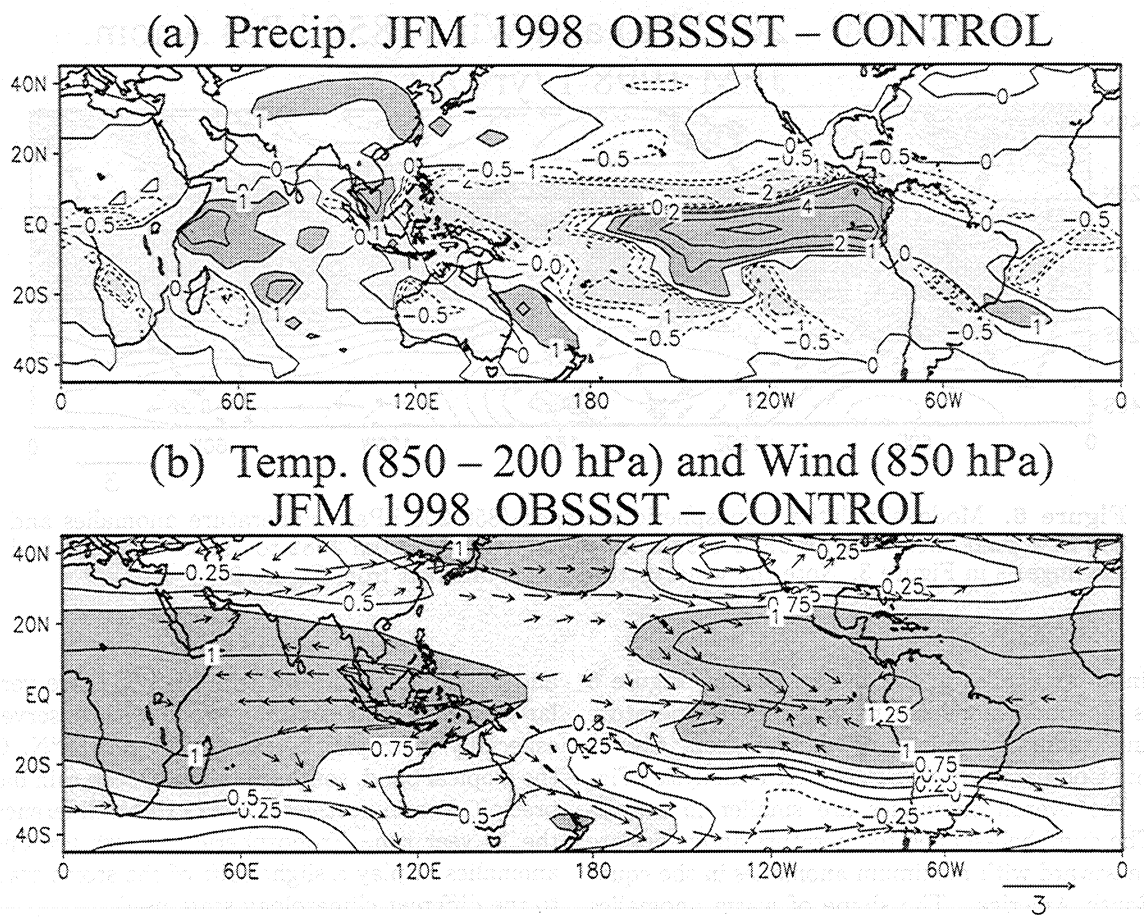

Figure 7. Model-simulated anomalies for JFM 1998 from the OBS-SST run (a) precipitation and (b) tropospheric temperature and 850 hPa wind anomalies. Contours and shadings for precipitation anomalies as in Figure 5. Tropospheric temperature contours and shadings and 850 hPa wind anomalies vector scale as in Figure 6.

ward into the western Indian Ocean. Within the warm temperature region, a low level easterly wind anomaly prevails to the east of a heat source and a westerly wind anomaly to the west. In the central and eastern Pacific, convergence is associated not only with the zonal wind anomalies but also with equatorward flow on both sides of the equator. Compared to Figure 7, the easterly anomaly to the east of the ENSO warm region is concentrated in the central and eastern Indian Ocean in run OBS-SST, suggesting that SST anomalies in other oceans modify the remote effect of the positive Pacific Ocean SST anomalies: compensating it in the western Indian Ocean and Africa and enhancing it in the eastern Indian Ocean and western Pacific.

Although cold SST anomalies in the Pacific are relatively small in both seasons, the NEGPAC run (Figure 9) shows that they generate substantial local negative precipitation anomalies. In JFM 1998 these cold SST anomalies noticeably enhance the relative subsidence induced by the POSPAC warm SST anomalies; and in some regions, they actually dominate the response. In the western Pacific and maritime continent, the local cold SST anomalies are the leading factor responsible for the reduction of rainfall (Figures 9a and 9c). *Nicholls* [1984] examined the relationship of ENSO to SST anomalies in the Indonesian region and postulated that zonal wind anomalies associated with the SST anomalies in the Indonesian region might be causes of certain aspects of the ENSO phenomenon. Recently, the role of cold SST anomalies and atmospheric anomalies in the western Pacific Ocean in the evolution of ENSO has been considered by *Weisberg and Wang* [1997a, 1997b], *Mayer and Weisberg* [1998], and *Wang et al.* [1999]. They proposed that the cold SST anomalies in the western Pacific produce equatorial easterly anomalies and that these wind anomalies in turn create feedbacks to the ocean and might affect ENSO evolution. In the NEGPAC run, the anomalous easterlies prevail in the far western Pacific and maritime continent (Figures 9b and 9d), extending into the Indian Ocean. We note that the overall magnitude of tropospheric temperature and wind anomalies is smaller than that of anomalies associated with the POSPAC warm SST anomalies. A separate feature of interest in the JFM 1998 NEGPAC run is that the center of cold tropospheric temperature anomalies is not colocated with the largest negative rainfall anomalies (Figure 9d). This is because tropospheric temperate change

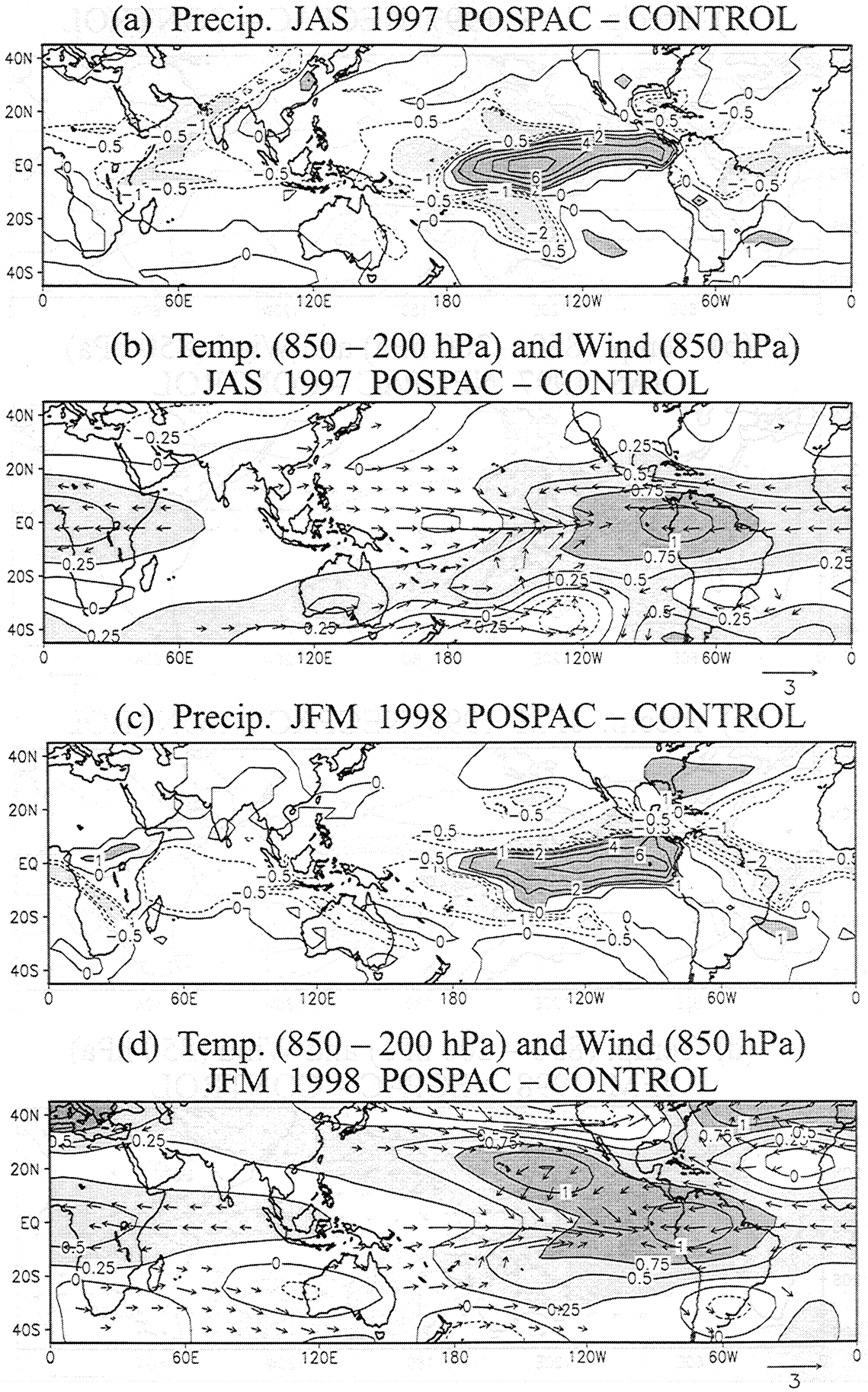

Figure 8. Model-simulated anomalies from the POSPAC run: (a) precipitation during JAS 1997, (b) tropospheric temperature and 850 hPa wind anomalies during JAS 1997, (c) precipitation during JFM 1998, and (d) tropospheric temperature and 850 hPa wind anomalies during JFM 1998. Contours, shadings and wind vector scale as in Figure 7.

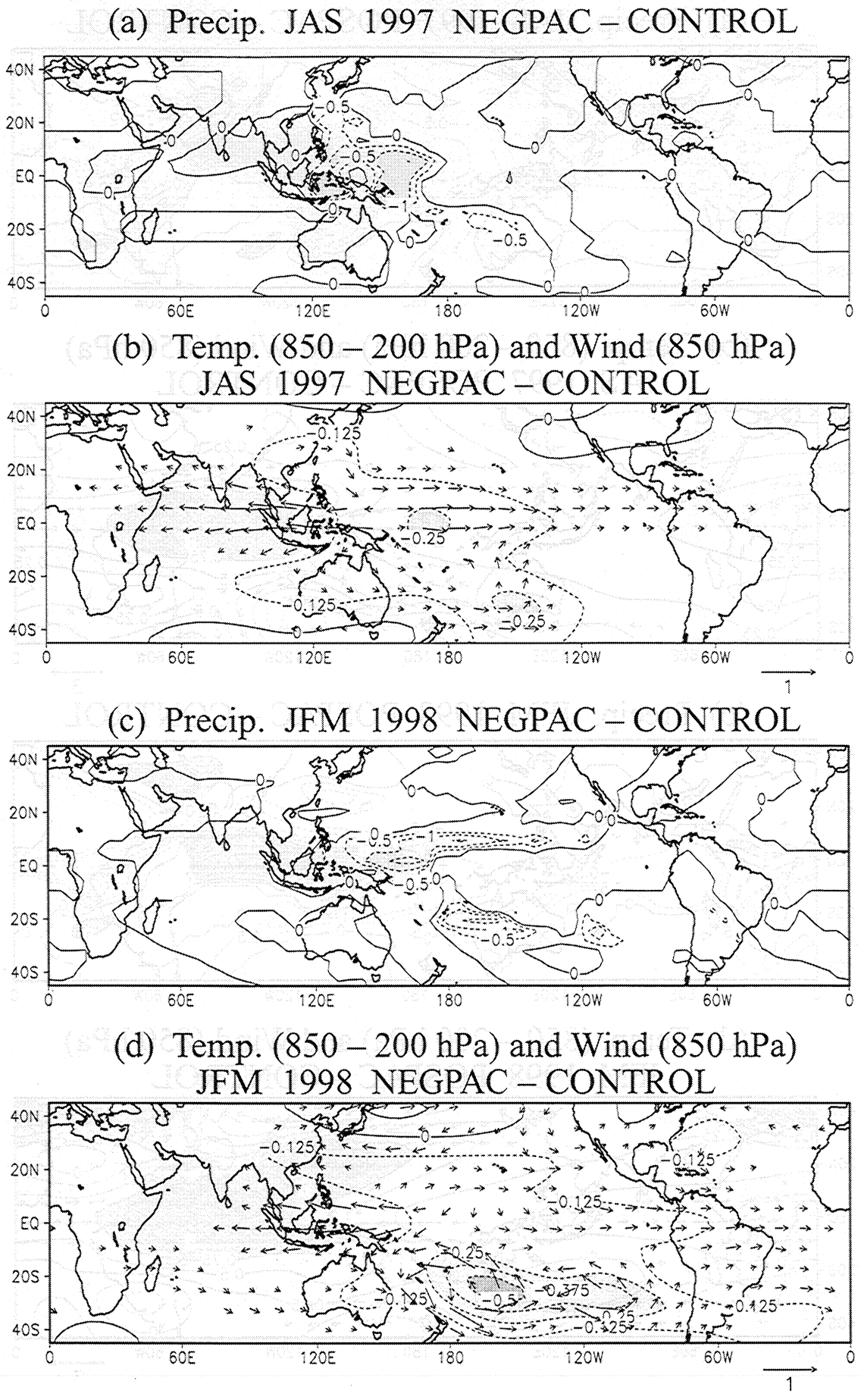

Figure 9. As in Figure 8 but for the NEGPAC run. Contour interval for precipitation anomalies is 0.5 mm d^{-1}, shaded below -1. Contour interval for temperature anomalies is 0.125°C, shaded below −0.25°C.

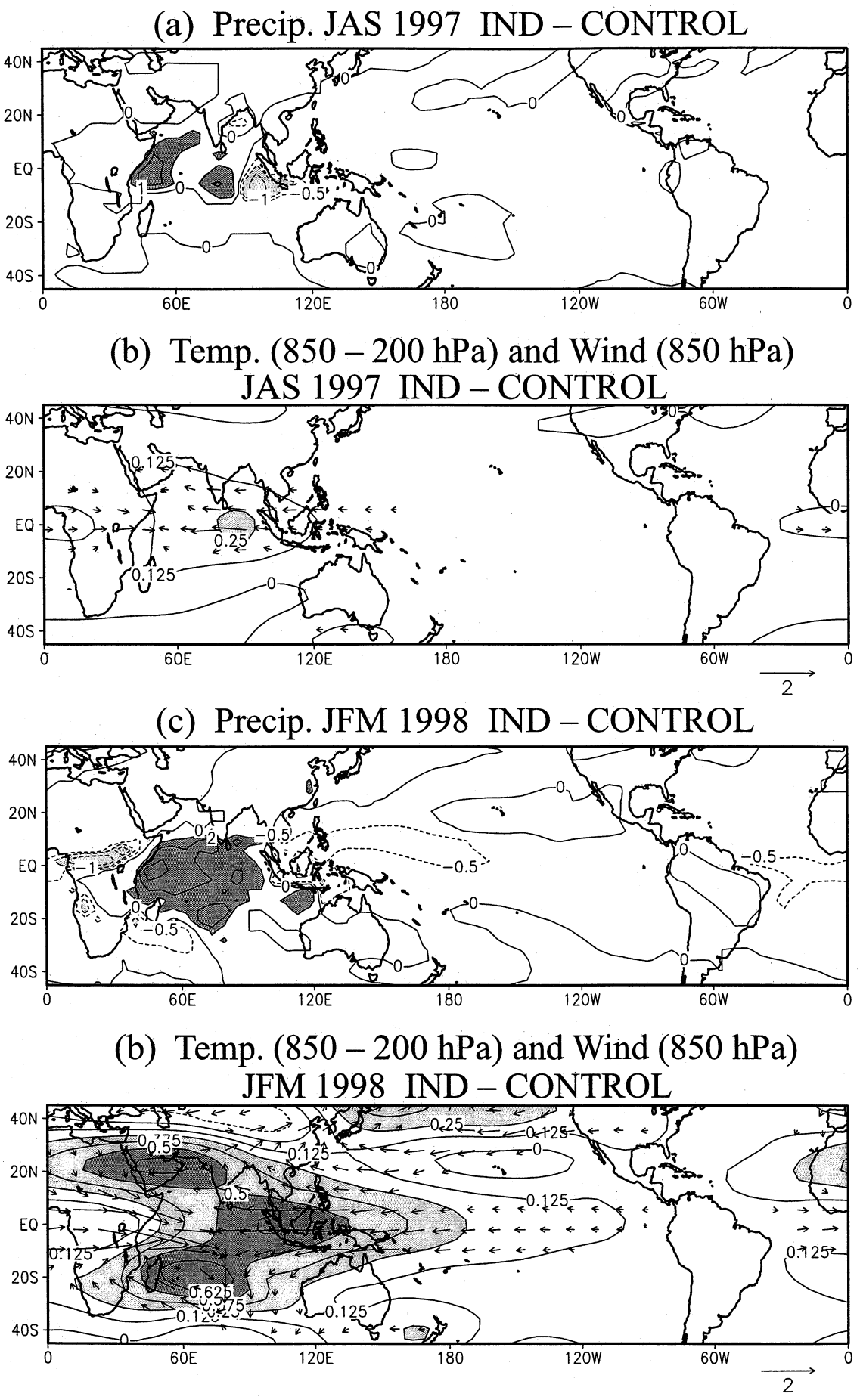

Figure 10. As in Figure 8 but for the IND run. Contour interval for precipitation anomalies is 0.5 mm d^{-1}, with dark shading above 1 and light shading below -1. Contour interval for temperature anomalies is 0.125°C, shaded above 0.25°C.

involves changes in advection and radiation and is not necessarily dominated by convective heating.

The effect of the Indian Ocean SST is seen in run IND (Figure 10). As noted in Figure 1a, during the summer of 1997, the Indian Ocean experienced moderate warming except in a relatively small area near Indonesia, where cooler than normal SST was observed. The precipitation response in Figure 10 is correlated with local SST anomalies, namely, rainfall is increased over regions of warmer SST and decreased in the colder SST regions (Figure 10a). Outside the basin, precipitation response is negligible. However, temperature and wind anomalies propagate much further. Sizable westerly anomalies spread across the African continent into the eastern Atlantic and easterly wind anomalies extend into the western Pacific (Figure 10b). In the winter of 1998 the Indian Ocean had a strong warming over the whole basin. In the model response (Figure 10c) this yields basin-wide enhanced rainfall in the Indian Ocean and induces less rainfall in the western Pacific and the equatorial Atlantic. The drying in the Indian Ocean and the Australian continent caused by teleconnection of positive SST anomalies in the Pacific Ocean, seen in Figure 8c, is partly canceled by the effect of warm SST anomalies in the Indian Ocean. The net precipitation anomalies in the Indian Ocean thus become positive, while negative precipitation anomalies in Australia are less extensive in Figure 7a than that in Figure 8c. Its impact over Africa is primarily reduction in rainfall along the equator and around 15°S in the western part of the continent. The positive precipitation anomalies in the eastern Africa is produced in run IND, although the magnitude is less than the observed anomalies of up to 2 mm d^{-1}. Compared to the OBS-SST run (Figure 7a), the Indian Ocean SST accounts for the largest part of the signal in this region. The teleconnected POSPAC SST response (Figure 8c) tends to cancel part of the equatorial signal and enhance the negative anomalies farther south.

Comparing the OBS-SST experiment (Figure 7a) to the anomaly from the 17 year run (Figure 5b) in this region, the features are generally similar, but the anomaly near 15°S is stronger and is less confined to the west in the 17 year run than that in run OBS-SST. The 17 year run, in turn, can be compared to the observations (Figure 2b). While the African simulation is far from perfect, missing dry anomalies around 10°S, the features of negative anomalies along the equator and in south central Africa, and the small penetration into the continent of the Indian Ocean positive anomalies are roughly comparable. *Latif et al.* [1999] performed similar Indian-only SST response experiments and found that the SST anomalies in the Indian Ocean were the primary factor responsible for the positive rainfall anomalies over the eastern equatorial Africa during the 1997-1998 El Niño and that the ENSO warm anomalies in the Pacific tend to counteract the effect of the Indian Ocean SST over Africa. We note that these results cannot be compared directly to *Goddard and Graham* [1999] since they examined November-December-January, when observed rainfall anomalies were very different. However, the present results concur with their conclusion that the Indian Ocean SST greatly affects rainfall in the eastern, central, and southern Africa. Interestingly, even though the spatial patterns differ between the two time periods, the tendency of teleconnections from the Pacific to cancel part of the signal due to the Indian Ocean occurs here as well as in Goddard and Graham's results.

Associated with the strong warming in the Indian Ocean during JFM 1998, tropospheric averaged temperature exhibits a significant warm anomaly in the eastern hemisphere. The maximum warming of tropospheric temperature surrounds the maximum warm SST in the western Indian Ocean, with a warm tongue protruding into the Pacific. A strong westerly wind anomaly at 850 hPa develops in the western Indian Ocean and Africa, while easterly wind anomalies prevail in the eastern Indian Ocean and western Pacific (Figure 10d).

Figure 11 shows the model response to the Atlantic SST anomaly associated with the 1997-1998 El Niño. In summer 1997 the tropical Atlantic Ocean had very small SST anomalies. Nonetheless, the weak cold SST anomalies on the equator yield a negative rainfall anomaly near the coast of Brazil and add to the drying caused by the teleconnection from the warm Pacific SST (figure not shown). Temperature and wind anomalies are very weak. During JFM 1998 the Atlantic experienced moderate warming. This generates increased rainfall in the equatorial Atlantic and counteracts the drought induced by the Pacific warm SST. It also has a remote influence on the convergence zone in central South America and Central America (Figure 11a). The corresponding anomalous warming in the tropospheric temperature and the anomalous wind field spread as far as to the western Pacific. In the western Indian Ocean and Africa, the Atlantic Ocean and the Pacific ENSO warm SST both produce easterly low-level wind anomalies, competing with the westerly anomalies associated with the anomalous SST in the Indian Ocean. The wind anomaly in run OBS-SST over these regions is thus weak due to cancelation among the Pacific, Atlantic, and local effects.

To examine the linearity of tropical response to SST anomalies, we compare combinations of the runs described above with SST anomalies specified in particular regions to the PAC, PACSTAR, and OBS-SST runs. The results of run PAC (with both positive and negative SST anomalies in the Pacific) look very similar to the sum of runs POSPAC and NEGPAC. Similarly, run PACSTAR resembles the sum of runs IND and ATL. Corresponding figures are not shown because they resemble other figures. However, in each case, there are departures from linearity that can be noted and they vary with region and season. For instance, considering the difference between runs PAC+PACSTAR and OBS-SST, in the summer of 1997, when SST anomalies are

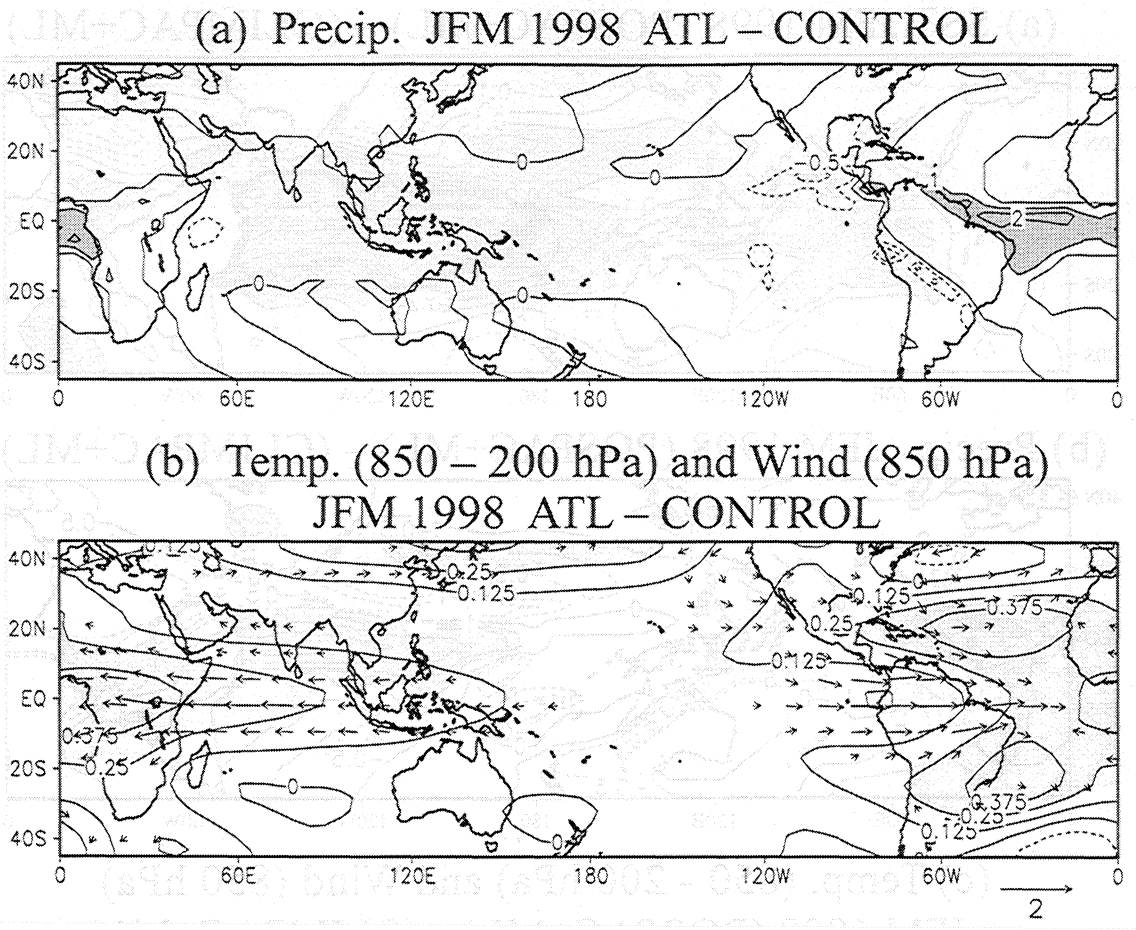

Figure 11. As in Figure 7 but for the ATL run. Contours, shading, and wind vector scale as Figure 10.

relatively weak outside the central ENSO warm region, departures from linearity are quite small. The area showing the strongest nonlinearity is northern South American where run PAC+PACSTAR has 20% less negative precipitation anomalies than run OBS-SST. During JFM 1998, nonlinear effects are evident in many regions. Departure from linearity as measured in the precipitation field occurs mostly in local regions, with a magnitude up to 0.4 mm d^{-1}. The deviation tends to occur in elongated bands but not always in the margins of strong anomaly regions. We do not find a consistent pattern regarding where the nonlinearity occurs, although regions exhibiting nonlinearity tend to be close to large anomalies. The nonlinearity does not appear solely due to saturation effects, i.e., the effect of two forcings acting together being less than the sum of the individual responses. For example, the OBS-SST run produces more reduction of rainfall in the western Pacific than the sum of PAC and PACSTAR. The effects in equatorial South America are similar. In the tropospheric temperature and wind anomaly fields, nonlinearity is mainly seen in extratropical storm tracks. Overall, nonlinearity is quantitatively important in particular regions. However, the effects are small enough that analyzing the results of SST anomalies in separate regions can give insight into the behaviors of the response as a whole.

3.3. Simulations With a Mixed-Layer Ocean Model

As shown in Figure 1, there were cold SST anomalies in the tropical Pacific surrounding the warm anomalies during both summer and the winter seasons of the 1997-1998 El Niño, as is the case in many events [*Wallace et al.*, 1998]. It is not clear whether the cold SST anomalies are caused by changes in surface fluxes in response to the strong warm anomalies or due to changes in ocean circulation. On the other hand, it is known that equatorial upwelling is confined to a narrow region near the equator. Whether surface fluxes are able to spread the warm SST anomalies to a wide area remains an open question. As a preliminary attempt to address these questions, we performed simulations with the combination of a mixed-layer ocean model and specified SST in regions of the warmest SST.

In Figure 12, run POSPAC+ML denotes the run with observed positive SST anomalies specified only in the central and eastern Pacific and a mixed-layer ocean that is active elsewhere. In contrast, run CLIMPAC+ML represents the control experiment in which climatologi-

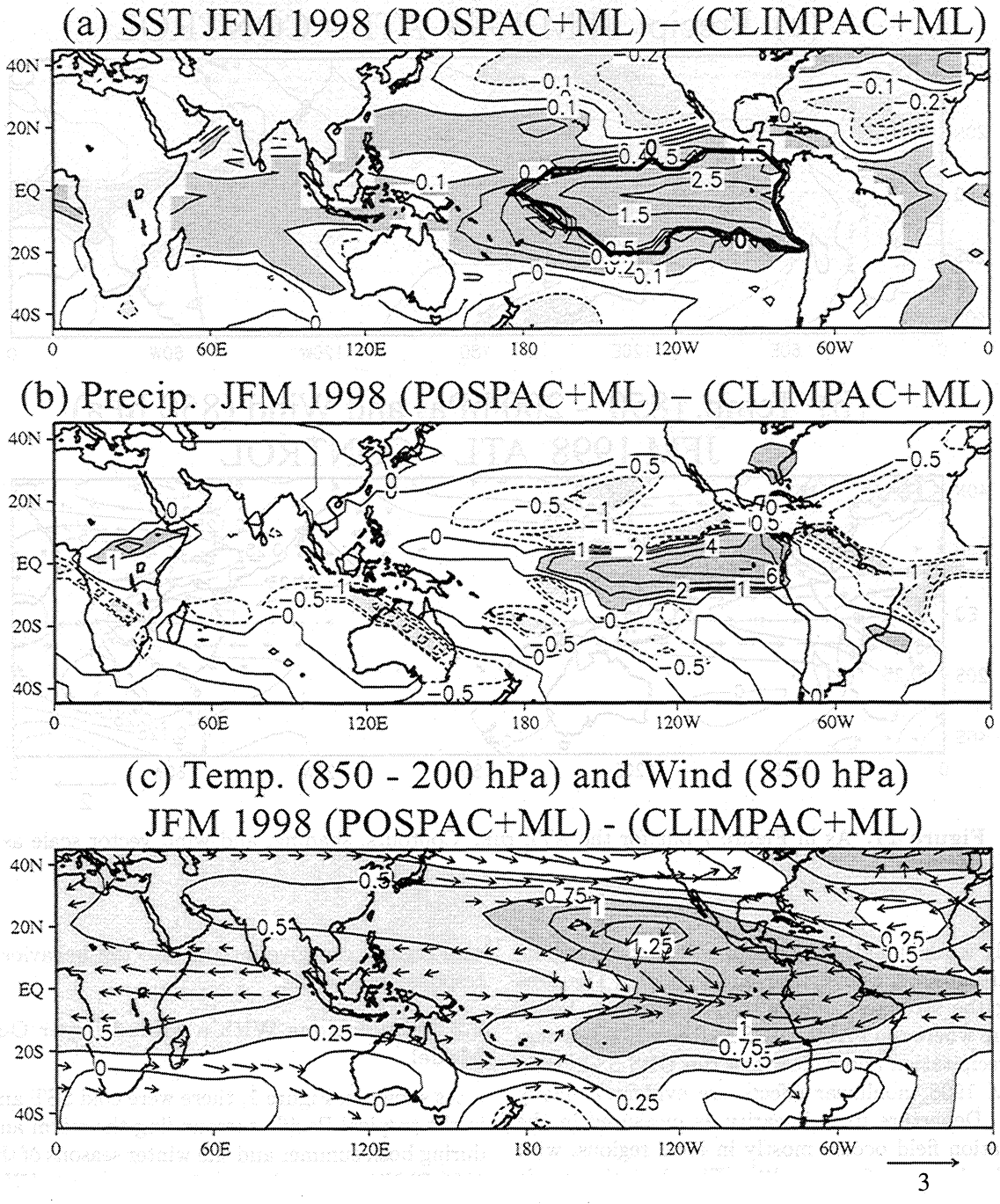

Figure 12. Model-simulated anomalies for JFM 1998 from the run POSPAC+ML - CLIMPAC+ML: (a) SST; (b) precipitation, and (c) tropospheric temperature and 850 hPa wind anomalies. SST contour interval is 0.1°C then 0.5°C after 0.5 contour. Dark shading above 0.1 and light shading below -0.1. Precipitation and temperature contours and shadings as in Figure 7.

cal SST replaces the POSPAC SST in the ENSO warm region. The simulated SST anomalies given by the difference POSPAC+ML minus CLIMPAC+ML during JFM 1998 are shown in Figure 12a. Compared to observed SST anomalies (Figure 1b), the changes in surface fluxes associated with atmospheric circulation do not produce the cold SST anomalies surrounding the warm SST within 20°S-20°N. The absence of the "horseshoe" pattern of cold SST anomalies in the central and western tropical Pacific suggests circumstantially that these are likely caused by changes in ocean circulation. It is known that the thermocline tends to shallow in these regions during an El Niño event. Although vertical advection is small in these regions, it is plausible that thermocline anomalies could affect sea surface temperature in the western Pacific via mixing processes. Although there are simulated cold SST anomalies north of 20°N across the north Pacific and

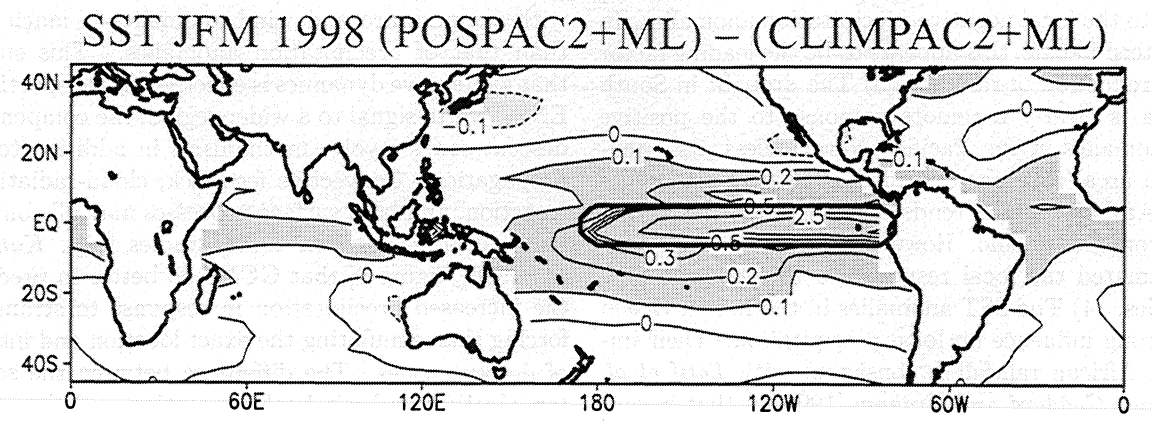

Figure 13. Model-simulated SST anomalies for JFM 1998 from the POSPAC2+ML - CLIMPAC2+ML. Contours and shadings as in Figure 12a.

south of 30°S near the dateline, they are not the focus of this paper since such effects have already been studied in models with more reliable midlatitude simulation [e.g., *Alexander,* 1992].

The distribution of tropospheric temperature and wind anomalies in the POSPAC+ML run is similar to that of the POSPAC run (Figure 12c). The negative precipitation anomalies (Figure 12b) to the north and south of the main ENSO-enhanced precipitation region are somewhat modified (larger magnitude at 20°N and smaller at 15°S).

Widespread SST warming occurs also in the Indian Ocean and equatorial Atlantic in run POSPAC+ML (Figure 12a), indicating a possible teleconnection from basin to basin via the "atmospheric bridge" [*Lau and Nath,* 1996; *Klein et al.,* 1999]. However, the amplitude of warming in the Indian Ocean and Atlantic is smaller than observed. A simulation by *Dommenget* [2000], using a variable depth mixed-layer model, which includes observed seasonal variation of a sub-mixed-layer term, produced greater amplitude of SST anomalies in the Indian Ocean. Besides the broad warming in the Indian basin, a relatively small area of cold SST anomalies in the eastern Indian Ocean is produced in the POSPAC+ML run. This is consistent with the observed reversed SST gradient in the Indian Ocean during the 1997-1998 ENSO event. Nevertheless, as noted by *Webster et al.* [1999] and *Yu and Rienecker* [2000], the substantial SST anomalies in the Indian Ocean during 1997-1998 may not be a direct response to the El Niño warming in the Pacific. It may rather represent the internal variability of the Indian Ocean climate system. At least one mechanism not included in the QTCM/mixed-layer model must have been active in observations. However, the system presented here indicates that some degree of interbasin teleconnection does occur.

The atmospheric circulation and associated surface heat fluxes appear to spread the warm anomalies in latitude in the eastern Pacific (Figure 12a). To further examine this latitudinal spreading in run POSPAC+ML, run POSPAC2+ML and run CLIMPAC2+ML were conducted, specifying SST only in the narrow strip of two grid boxes near the equator. POSPAC2+ML uses observed SST anomalies in that region, whereas climatological SST is used in CLIMPAC2+ML. Figure 13 shows that the warm SST anomalies are seen across the tropical Pacific within 20°. The amplitude is generally smaller in particular regions than that in Figure 12a, showing that the width of warm SST anomalies in addition to the magnitude of warm anomalies affects the response to El Niño. The run confirms that changes in air-sea heat fluxes associated with atmospheric teleconnection can help to spread warming roughly 10°-15° north and south from the region most directly affected by equatorial upwelling. However, since the observed warming off the equator in the eastern Pacific is larger than that which is reproduced in the mixed-layer model, oceanic processes must also play a role.

4. Summary and Conclusions

The quasi-equilibrium tropical circulation model is used to explore the tropical response to SST anomalies during the 1997-1998 El Niño event. The model simulates the observed precipitation anomalies during both the summer and the winter seasons of this event. Exceptions include the following: The model tends to produce less areal coverage of drought in South America than observations, the reduction of rainfall over the eastern Indian Ocean is underestimated, and the modeled enhanced precipitation in the central and eastern Pacific extends less westward than observations. Tropospheric temperature and wind anomalies broadly resemble the NCEP/NCAR reanalysis but with smaller magnitude.

Particular conclusions, based on the model results of regional SST experiments, include the following: (1) The negative precipitation anomalies to the north and south of the enhanced precipitation region in the Pacific are mainly a response to the ENSO warm SST anomalies. (2) The cold SST anomalies in the Pacific con-

tribute to the local negative precipitation anomalies. In the western Pacific, this appears to be the leading factor for the reduction of rainfall. (3) The drought in South America is clearly a remote response to the positive SST anomalies in the Pacific. Nevertheless, its intensity and areal coverage are affected by SST anomalies in the Atlantic, which tends to counteract the drying effect from the Pacific. However, the model may have overestimated the local response to the Atlantic SST anomalies. (4) The SST anomalies in the Indian Ocean have strong influence on local precipitation. Their impact on African rainfall is consistent with *Latif et al.* [1999] and *Goddard and Graham* [1999] in that it cancels the remote effect of warm SST in the Pacific and creates drought in equatorial Africa. The Indian Ocean SST anomalies also contribute to the negative rainfall anomalies in southwestern Africa in addition to the Pacific effects.

The simulations with a combination of a mixed-layer ocean model and localized SST anomalies suggest that cold SST anomalies surrounding the strong ENSO warm region are not produced by surface heat flux changes associated with atmospheric circulation. A reasonable inference is that these cold anomalies may be caused by changes in oceanic circulation. In the eastern Pacific the atmosphere can contribute modestly to spreading SST anomalies latitudinally. The atmosphere, via surface heat flux effects, tends to spread El Niño warm anomalies from a confined area to a much wider region. Teleconnection from the Pacific to the Indian Ocean produces about one fifth of the observed warm anomalies in the Indian Ocean. The reversed SST gradient in the Indian basin is also produced by the model. Obviously, the coupling to a mixed-layer ocean omits other mechanisms, such as internal variability and ocean dynamical feedbacks, which can produce anomalies in other regions [*Webster et al.* 1999]. This system does provide confirmation that teleconnection from the El Niño warm region can affect other regions via surface heat fluxes [*Klein et al.* 1999], although this model suggests such anomalies are modest. The results suggest that a tendency toward warming in other parts of the tropical Pacific and in the Indian Ocean is a relatively simple aspect of the teleconnection to capture, since it is found in this system.

In both the regional specified SST experiments and mixed-layer experiments, a comparison of the pattern of precipitation anomalies with that of tropospheric temperature and wind anomalies shows that while the negative precipitation anomalies tend to occur within the convective zones and relatively near the positive SST anomalies, tropospheric temperature and wind anomalies extend much further from basin to basin. The spatial pattern of temperature tends to be much smoother than that of precipitation. Negative precipitation anomalies, associated with descent anomalies, do not appear to be related to temperature and wind anomalies in a simple manner. The teleconnection scale associated with temperature and wind anomalies is much larger than that of precipitation anomalies. This suggests that while wave dynamics is effective in transporting the ENSO warm signal to a wider region, the compensating descent zones involve mechanisms in addition to wave propagation. Convective feedback, cloud-radiation interaction, and land surface processes may all come into play. It appears from GCM studies [e.g., *Kumar et al.*, 1996, Figure 9] that GCMs do better in predicting the increased precipitation in response to strong SST forcing than simulating the exact location and intensity of descent zones. The difference between the scale of temperature and wind teleconnection and the scale of precipitation teleconnection may be an indication of the complexity of descent zone simulation.

Acknowledgments. This work was supported in part by National Science Foundation grant ATM-0082529, National Oceanographic and Atmospheric Administration grant NA86-GP0314, and National Aeronautics and Space Administration grant NA G5-9358. This is UCLA IGPP contribution 5640. The authors thank J. E. Meyerson for graphical assistance. Comments from M. Munnich and N. Zeng are greatly appreciated.

References

Alexander, M. A., Midlatitude atmosphere-ocean interaction during El Niño, part I, The North Pacific Ocean, *J. Clim.*, *5*, 944-958, 1992.

Barnett, T. P., et al., Forecasting global ENSO-related climate anomalies, *Tellus, Ser. A 46*, 381-397, 1994.

Barnston, A. G., M. H. Glantz, and Y. He, Predictive skill of statistical and dynamical climate models in SST forecasts during the 1997-98 El Nino episode and the 1998 La Nina onset, *Bull. Am. Meteorol. Soc., 80*, 217-243, 1999a.

Barnston, A. G., A. Leetmaa, V. E. Kousky, R. E. Livezey, E. A. O'Lenic, H. V. den Dool, A. J. Wagner, and D. A. Unger, NCEP Forecasts of the El Niño of 1997-98 and its U.S. impacts, *Bull. Am. Meteorol. Soc., 80*, 1829-1852, 1999b.

Chang, P., R. Saravanan, L. Ji, and G. C. Hegerl, The effect of local sea surface temperatures on atmospheric circulation over the tropical Atlantic sector, *J. Clim., 13*, 2195-2216, 2000.

Chou, C., J. D. Neelin, and H. Su, Ocean-atmosphere-land feedbacks in an idealized monsoon, *Q. J. R. Meteorol. Soc., in press*, 2001.

Dommenget, D., Large-scale SST variability in the midlatitudes and in the tropical Atlantic, Ph.D. thesis, Examensarb. 76, Max Planck Inst. for Meteorol., Hamburg, Germany, 2000.

Farrara, J. D., C. R. Mechoso, and A. W. Robertson, Ensembles of AGCM two-tier predictions and simulations of the circulation anomalies during winter 1997-98, *Mon. Weather Rev., 128*, 3589-3604, 2000.

Folland, C. K., T. N. Palmer and D. E. Parker, Sahel rainfall and worldwide sea temperatures, 1901-85, *Nature, 320*, 602-607, 1986.

Frederiksen, C. S., H. Zhang, R. C. Balgovind, N. Nicholls, W. Drosdowsky, and L. Chambers, Dynamical seasonal forecasts during the 1997/98 ENSO using persisted SST anomalies, *J. Clim., accepted*, 2001.

Gill, A. E., Some simple solutions for heat induced tropical circulation, *Q. J. R. Meteorol. Soc., 106*, 447-462, 1980.

Goddard, L., and N. E. Graham, The importance of the

Indian Ocean for simulating rainfall anomalies over eastern and southern Africa, *J. Geophys. Res.*, *104*, 19,099-19,116, 1999.

Halpert, M. S., and C. F. Ropelewski, Surface temperature patterns associated with the Southern Oscillation, *J. Clim.*, *5*, 577-593, 1992.

Hansen, J., I. Fung, A. Lacis, D. Rind, S. Lenedeff, R. Ruedy, and G. Russell, Global climate changes as forecast by Goddard Institute for Space Studies three-dimensional model, *J. Geophys. Res.*, *93*, 9341-9364, 1988.

Hansen, J., R. Ruedy, A. Lacis, G. Russell, M. Sato, J. Lerner, D. Rind, and P. Stone, Wonderland climate model, *J. Geophys. Res.*, *102*, 6823-6830, 1997.

Janicot, S., A. Harzallah, B. Fontaine, and V. Moron, West African monsoon dynamics and eastern equatorial Atlantic and Pacific SST anomalies (1970-88), *J. Clim.*, *11*, 1874-1882, 1998.

Kalnay, E., et al., The NCEP/NCAR 40-year reanalysis project, *Bull. Am. Meteorol. Soc.*, *77*, 437-471, 1996.

Klein, S., B. J. Soden, and N.-C. Lau, Remote sea surface temperature variations during ENSO: Evidence for a tropical atmospheric bridge, *J. Clim.*, *12*, 917-932, 1999.

Kumar, A., M. Hoerling, M. Ji, A. Leetmaa, and P. Sardeshmukh, Assessing a GCM's suitability for making seasonal predictions, *J. Clim.*, *9*, 115-129, 1996.

Kumar, A., and M. P. Hoerling, Specification of regional sea surface temperatures in the atmospheric general circulation model simulations, *J. Geophys. Res.*, *103*, 8901-8907, 1998.

Latif, M., D. Dommenget, M. Dima, and A. Grotzner, The role of Indian Ocean sea surface temperature in forcing east African rainfall anomalies during December-January 1997/98, *J. Clim.*, *12*, 3497-3504, 1999.

Lau, N.-C., Modeling the seasonal dependence of the atmospheric response to observed El Niños in 1962-76, *Mon. Weather Rev.*, *113*, 1970-1996, 1985.

Lau, N. C., and M. J. Nath, The role of the "atmospheric bridge" in linking tropical Pacific ENSO events to extratropical SST anomalies, *J. Clim.*, *9*, 2036-2057, 1996.

Lin, J. W.-B., and J. D. Neelin, Influence of a stochastic moist convective parameterization on tropical climate variability, *Geophys. Res. Lett.*, *27*, 3691-3694, 2000.

Lin, J. W.-B., J. D. Neelin, and N. Zeng, Maintenance of tropical intraseasonal variability: Impact of evaporation-wind feedback and mid-latitude storms, *J. Atmos. Sci.*, *57*, 2793-2823, 2000.

Mayer, D. A., and R. H. Weisberg, El Niño-Southern Oscillation related ocean-atmosphere coupling in the western equatorial Pacific, *J. Geophys. Res.*, *103*, 18,635-18,648, 1998.

Mechoso, C. R., A. Kitoh, S. Moorthi, and A. Arakawa, Numerical simulations of the atmospheric response to a sea surface temperature anomaly over the equatorial eastern Pacific Ocean, *Mon. Weather Rev.*, *115*, 2936-2956, 1987.

Neelin, J. D. and N. Zeng, A quasi-equilibrium tropical circulation model—Formulation, *J. Atmos. Sci.*, *57*, 1741-1766, 2000.

Nicholls, N., The southern oscillation and Indonesian sea surface temperature, *Mon. Weather Rev.*, *112*, 424-432, 1984.

Palmer, T. N., Influence of the Atlantic, Pacific and Indian Oceans on Sahel rainfall, *Nature*, *322*, 251-253, 1986.

Quinn, W., D. Zopf, K. Short, and R. Yang, Historical trends and statistics of the Southern Oscillation, El Niño, and Indonesian drought, *Fish. Bull.*, *76*, 663-678, 1978.

Reynolds, R. W., and T. M. Smith, Improved global sea surface temperature analyses using optimum interpolation, *J. Clim.*, *7*, 929-948, 1994.

Ropelewski, C. F., and M. S. Halpert, Global and regional scale precipitation associated with El Niño/Southern Oscillation, *Mon. Weather Rev.*, *115*, 1606-1626, 1987.

Rowell, D., Assessing potential seasonal predictability with an ensemble of multidecadal GCM simulations, *J. Clim.*, *11*, 109-120, 1998.

Saravanan, R., and P. Chang, Interaction between tropical Atlantic variability and El Niño–Southern Oscillation, *J. Clim.*, *13*, 2177- 2194, 2000.

Sud, Y. C., G. K. Walker, and W. E. Smith, Analysis of a general circulation model simulation of the atmospheric response to the observed sea surface temperature anomalies of January and February 1983, *J. Clim.*, *4*, 107-115, 1991.

Trenberth, K. E., G. W. Branstator, D. Karoly, A. Kumar, N.-C. Lau, and C. Ropelewski, Progress during TOGA in understanding and modeling global teleconnections associated with tropical sea surface temperatures, *J. Geophys. Res.*, *103*, 14,291-14,324, 1998.

Venzke, S., M. Latif, and A. Villwock, The Coupled GCM ECHO-2, part II, Indian Ocean response to ENSO, *J. Clim.*, *13*, 1371-1383, 2000.

Wallace, J. M., E. M. Rasmusson, T. P. Mitchell, V. E. Kousky, E. S. Sarachik, and H. von Storch, On the structure and evolution of ENSO-related climate variability in the tropical Pacific: Lessons from TOGA, *J. Geophys. Res.*, *103*, 14,241–14,260, 1998.

Wang, C., R. H. Weisberg, and J. I. Virmani, Western Pacific interannual variability associated with the El Niño-Southern Oscillation, *J. Geophys. Res.*, *104*, 5131-5149, 1999.

Webster, P. J., A. M. Moore, J. P. Loschnigg, and R. R. Leben, Coupled ocean-atmosphere dynamics in the Indian Ocean during 1997-98, *Nature*, *401*, 356-360, 1999.

Weisberg, R. H., and C. Wang, Slow variability in the equatorial west-central Pacific in relation to ENSO, *J. Clim.*, *10*, 1998-2017, 1997a.

Weisberg, R. H., and C. Wang, A western Pacific oscillator paradigm for the El Niño-Southern Oscillation, *Geophys. Res. Lett.*, *24*, 779-782, 1997b.

Xie, P., and P.A. Arkin, Global precipitation: A 17-year monthly analysis based on gauge observations, satellite estimates and numerical model outputs, *Bull. Am. Meteorol. Soc.*, *78*, 2539-2558, 1997.

Yu, L., and M. M. Rienecker, Indian Ocean warming of 1997-1998, *J. Geophys. Res.*, *105*, 16,923-16,939, 2000.

Yulaeva, E., and J. M. Wallace, The signature of ENSO in global temperature and precipitation fields derived from the microwave sounding unit, *J. Clim.*, *7*, 1719-1736, 1994.

Zeng, N., J. D. Neelin, and C. Chou, A quasi-equilibrium tropical circulation model-implementation and simulation, *J. Atmos. Sci.*, *57*, 1767-1796, 2000.

C. Chou, J. D. Neelin, and H. Su, Department of Atmospheric Sciences, University of California, Los Angeles, 405 Hilgard Ave., Los Angeles, CA 90095-1565. (chia@atmos.ucla.edu; neelin@atmos.ucla.edu; hui@atmos.ucla.edu)

(Received November 6, 2000; revised March 27, 2001; accepted March 27, 2001.)